Selective excitation in a three-state system using a hybrid adiabatic-nonadiabatic interaction

Yunheung Song, Han-gyeol Lee, Hanlae Jo, and Jaewook Ahn
Department of Physics, KAIST, Daejeon 305-701, Korea
(Received 14 April 2016; published 18 August 2016)

The chirped-pulse interaction in the adiabatic coupling regime induces cyclic permutations of the energy states of a three-level system in the V-type configuration, which process is known as the three-level chirped rapid adiabatic passage (RAP). Here we show that a spectral hole in a chirped pulse can turn on or off the level mixing at adiabatic crossing points of this process, reducing the system to an effective two-level system. The given hybrid adiabatic-nonadiabatic transition enables selective excitation of the three-level system, controlled by the laser intensity and spectral position of the hole, as well as the sign of the chirp parameter. Experiments performed with shaped femtosecond laser pulses and the three lowest energy levels ($5S_{1/2}$, $5P_{1/2}$, and $5P_{3/2}$) of atomic rubidium (^{85}Rb) show good agreement with the theoretically analyzed dynamics. The result indicates that our method, when being combined with the ordinary chirped RAP, implements an adiabatic transition between the Raman-coupled excited states. Furthermore, our laser intensity-dependent control may have applications including selective excitations of atoms or ions arranged in space when being used in conjunction with laser beam profile programming.

DOI: 10.1103/PhysRevA.94.023412

I. INTRODUCTION

Adiabatic control of a quantum system through its adiabatic evolution path allows robust manipulation and high-fidelity state preparation [1]. Gradually being recognized as an important requirement in quantum information processing [2], it has been under active investigation in recent years [3–9]. The best known examples of the adiabatic control methods are the rapid adiabatic passage (RAP) [10–12] and the stimulated Raman adiabatic passage [13]. Both of these methods have been widely applied to various quantum systems including atom optics [14], NMR [15], cavity quantum electrodynamics [16], superconducting qubits [17], and quantum dots [18].

Broadband light sources greatly benefit optical approaches to qubit manipulations because of their powerful pulse-shape programming capability [19,20]. In ultrafast optics, composing the amplitude and phase of a broadband laser pulse provides various complex pulse shapes, and their usage often plays a crucial role in investigating and engineering new quantum dynamics of atoms and molecules [21–26]. Of particular relevance in the context of the present paper is the selective population method of dressed states [26] which provides a pulse shaping scheme especially in the frequency domain for strong-field controls of multilevel systems.

In this paper we consider a laser pulse shaping method to embed a local nonadiabatic coupling in the middle of a three-level chirped RAP process [11,12]. The chirped RAP makes a set of cyclic permutation transitions for a three-level system in the V-type configuration: $|0\rangle \rightarrow |1\rangle$, $|1\rangle \rightarrow |0\rangle \rightarrow |2\rangle$, and $|2\rangle \rightarrow |0\rangle$ (for a positive chirp, and a negative chirp reverses the directions), when $|1\rangle$ and $|2\rangle$ are the excited states and $|0\rangle$ is the ground state. At the first and second adiabatic crossing points the state $|0\rangle$ is interchanged with $|1\rangle$ and $|2\rangle$, respectively. So if the transition at the first adiabatic crossing is turned off (with the new nonadiabatic coupling), the states $|0\rangle$ and $|1\rangle$ bypass the crossing, and the states $|0\rangle$ and $|2\rangle$ are interchanged at the second crossing and the state $|1\rangle$ is unchanged (i.e., $|0\rangle \rightarrow |2\rangle$, $|1\rangle \rightarrow |1\rangle$, and $|2\rangle \rightarrow |0\rangle$). We will show that this type of hybrid adiabatic-nonadiabatic interaction can be implemented with a chirped optical pulse with a *spectral hole* resonant to one of the two excited states. In our method the laser intensity is used to turn on or off the nonadiabatic coupling, while in a conventional RAP approach the spectral chirp sign is used for the selectivity [11,12]. Using the laser intensity as a control parameter brings along the benefit of spatial beam shaping, which enables simultaneous control of multiple qubits arranged in space (to be discussed as an application).

The remaining sections are organized as follows: We first theoretically study the model Hamiltonian for the given shaped-pulse interaction with a three-level system in Sec. II, where we show that the chirped pulse with a spectral hole can embed the nonadiabatic coupling amid a conventional RAP process. After the experimental procedure is briefly illustrated in Sec. III, the experimental results are provided in Sec. IV, where the intensity-dependent selectivity of the as-designed hybrid adiabatic-nonadiabatic interaction is presented. The conclusion follows in Sec. V.

II. THEORETICAL CONSIDERATION

The model system is a three-level atom in the V-type configuration, consisting of two excited energy states, $|1\rangle$ and $|2\rangle$, and the ground state, $|0\rangle$ (of respective energies $\hbar\omega_1$, $\hbar\omega_2$, and 0). We consider this system is interacted with a spectrally shaped laser pulse, a chirped Gaussian pulse with a spectral hole, defined in the spectral domain as

$$E(\omega) = E_0(e^{-(\omega-\omega_m)^2/\Delta\omega_m^2} - \alpha e^{-(\omega-\omega_h)^2/\Delta\omega_h^2})e^{-ic_2(\omega-\omega_m)^2/2}, \tag{1}$$

where ω_m and ω_h are the center frequencies of the main pulse and the hole, respectively, $\Delta\omega_m$ and $\Delta\omega_h$ are the bandwidths, and c_2 is the chirp parameter [19]. The condition $\alpha = \exp[-(\omega_h - \omega_m)^2/\Delta\omega_m^2]$ in Eq. (1) makes a complete spectral hole around $\omega = \omega_h$. The electric field in the time domain is the inverse Fourier transform of $E(\omega) + E(-\omega)$,

which is given by

$$E(t) = \frac{\mathcal{E}_m(t)}{2} e^{i\{(\omega_m+\beta_m t)t+\varphi_m\}} - \frac{\mathcal{E}_h(t)}{2} e^{i\{\omega_h+\beta_h(t-\gamma)\}(t-\gamma)+\varphi_h\}} + \text{c.c.} \equiv E_m(t) + E_h(t) + \text{c.c.}, \quad (2)$$

where $\beta_m = c_2/(2c_2^2 + 8/\Delta\omega_m^4)$ and $\beta_h = c_2/(2c_2^2 + 8/\Delta\omega_h^4)$ are the chirp parameters for the main and hole pulses, respectively, and $\gamma = -c_2(\omega_m - \omega_h)$ is the time shift of the hole with respect to the main pulse. The amplitudes and (time-independent) phases of the pulses are respectively given by

$$\mathcal{E}_m(t) = E_0\sqrt{\frac{\Delta\omega_m}{\tau_m}} e^{-t^2/\tau_m^2}, \quad (3)$$

$$\varphi_m = -\frac{1}{2}\tan^{-1}\frac{c_2\Delta\omega_m^2}{2}, \quad (4)$$

$$\mathcal{E}_h(t) = \alpha E_0\sqrt{\frac{\Delta\omega_h}{\tau_h}} e^{-(t-\gamma)^2/\tau_h^2}, \quad (5)$$

$$\varphi_h = -\frac{1}{2}\tan^{-1}\frac{c_2\Delta\omega_h^2}{2} - \frac{c_2}{2}\left(\omega_m^2 - \omega_h^2\right), \quad (6)$$

where $\tau_i = \sqrt{4/\Delta\omega_i^2 + c_2^2\Delta\omega_i^2}$ is the Gaussian pulse width of each chirped pulse $i = m,h$.

Suppose that the main pulse is frequency centered between the excited states [i.e., $\omega_m = (\omega_1 + \omega_2)/2$], with a bandwidth enough to cover both states (i.e., $\Delta\omega_m > \delta \equiv \omega_2 - \omega_1$) and that the hole pulse is resonant to only one of them, say, $|1\rangle$ (i.e., $\omega_h = \omega_1$ and $\Delta\omega_h < \delta$). The Hamiltonian is then given in the eigenstate basis by

$$H(t) = \begin{bmatrix} e_0(t) & 0 & 0 \\ 0 & e_1(t) & 0 \\ 0 & 0 & e_2(t) \end{bmatrix} - i\hbar R\dot{R}^{-1}, \quad (7)$$

where $\{e_j(t)\}$ are the eigenstate energies and $R_{jk}(t) = \langle e_j|k\rangle$ is the transformation from the bare basis $\{|k\rangle\}$ to the eigenstate basis $\{|e_j\rangle\}$ for $j,k \in \{0,1,2\}$. The time evolution of the eigenenergies $e_j(t)$ is plotted in Fig. 1(a), where we use $\Delta\omega_m = 10\Delta\omega_h = 2.5\delta$, and a positive $c_2 = 2/\Delta\omega_h^2$ is chosen to satisfy the minimum hole pulse-width condition for a constant chirp parameter. The main pulse induces slowly varying adiabatic passages (the dotted lines) and the hole the rapid change of them (the solid lines) near the first adiabatic crossing point. These behaviors are consistent with the temporal profiles of the main pulse and the hole, as shown in Fig. 1(b). Note that the instantaneous frequency of the main pulse becomes equal to ω_1 at $t = \gamma$.

(i) Fully adiabatic coupling regime. When the nonadiabatic coupling term, $-i\hbar R\dot{R}^{-1}$ in Eq. (7), is small, the adiabatic condition [10] is satisfied in all time. Each eigenstate $|e_i\rangle$ is an adiabatic state, evolving from one bare state $|i\rangle$ to the next one $|i+1\rangle$ (cyclically), i.e.,

$$\lim_{t\to-\infty}|e_0(t)\rangle = |0\rangle, \quad \lim_{t\to\infty}|e_0(t)\rangle = |1\rangle,$$
$$\lim_{t\to-\infty}|e_1(t)\rangle = |1\rangle, \quad \lim_{t\to\infty}|e_1(t)\rangle = |2\rangle,$$
$$\lim_{t\to-\infty}|e_2(t)\rangle = |2\rangle, \quad \lim_{t\to\infty}|e_2(t)\rangle = |0\rangle, \quad (8)$$

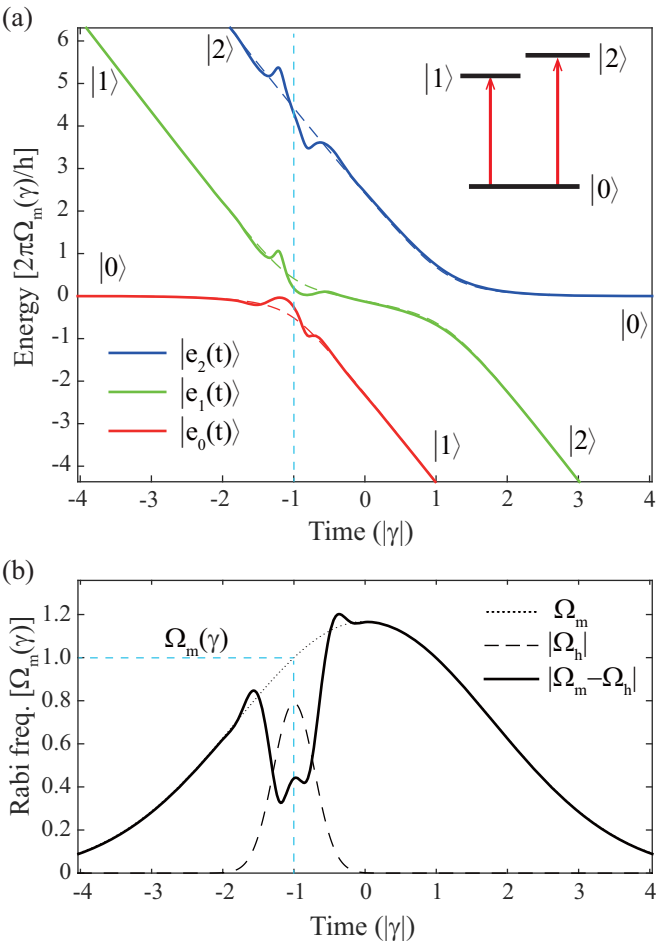

FIG. 1. (a) The time evolution of the eigenstate energies, $e_0(t)$, $e_1(t)$, and $e_2(t)$, of the V-type system Hamiltonian, including (solid lines) and excluding (dashed lines) the hole pulse interaction. (b) The temporal envelopes of the total pulse (solid line, $|\Omega_m - \Omega_h|$), the main pulse (dotted pulse, Ω_m), and the hole pulse (dashed line, $|\Omega_h|$), represented in $\Omega_m(\gamma)$ unit.

up to a global phase. (A negative chirp reverses the direction of the three-state cyclic permutation.) So, the result in the fully adiabatic three-state coupling regime is a cyclic transition ($|0\rangle \to |1\rangle$, $|1\rangle \to |2\rangle$, $|2\rangle \to |0\rangle$), similar to the three-level chirped RAP [11,12].

(ii) Hybrid adiabatic-nonadiabatic coupling regime. When the adiabatic condition is violated due to the presence of the hole (we consider the main pulse alone is still adiabatic), the given Hamiltonian results in a hybrid adiabatic-nonadiabatic transition between $|e_0\rangle$ and $|e_1\rangle$. Since the nonadiabatic coupling is localized in time near $t = \gamma$, we may consider two separate time regions: $t > 0$ and $t < 0$. In the positive time region, the dynamics is a fully adiabatic process, so the state at $t = 0$ simply remains until $t = \infty$. In the negative time region, the eigenstate $|e_2\rangle$ can be decoupled because it is far-off resonant from $|e_0\rangle$. When we rewrite the Hamiltonian in the adiabatic basis of the main pulse (only), the Hamiltonian is given under the rotating-wave

approximation by

$$H'(t<0)=\begin{bmatrix} e_-(t) & 0 & 0 \\ 0 & e_+(t) & 0 \\ 0 & 0 & 2\delta+\Delta(t) \end{bmatrix} - \frac{\hbar}{2}R'\begin{bmatrix} 0 & \Omega_h(t) & 0 \\ \Omega_h^*(t) & 0 & 0 \\ 0 & 0 & 0 \end{bmatrix}R'^{-1}, \quad (9)$$

where $e_\pm(t)=\hbar[\Delta(t)\pm\sqrt{\Omega_m(t)^2+\Delta(t)^2}]/2$ are the adiabatic energies, $\Delta(t)=-\delta-2\alpha t$ is the detuning (for the main pulse), and $R'(t)$ is the transform matrix given by

$$R'(t)=\begin{bmatrix} \cos\vartheta(t) & -\sin\vartheta(t) & 0 \\ \sin\vartheta(t) & \cos\vartheta(t) & 0 \\ 0 & 0 & 1 \end{bmatrix}, \quad (10)$$

with the mixing angle

$$\vartheta(t)=\frac{1}{2}\tan^{-1}\frac{\Omega_m(t)}{\Delta(t)} \quad \text{for} \quad 0\leqslant\vartheta(t)\leqslant\frac{\pi}{2}. \quad (11)$$

The Rabi frequency for the transition from $|0\rangle$ to $|1\rangle$ is defined by $\Omega_i(t)=2\mu_{01}E_i(t)\exp[-i(\alpha t^2+\omega_m t+\phi_m)]/\hbar$ for each pulse $i=m,h$, where the phase factor of the main pulse is added to keep Ω_m real.

The Hamiltonian in Eq. (9) can be simplified to be

$$H_F(t)=\hbar\begin{bmatrix} -\Delta_F(t)/2 & \Omega_F(t)/2 & 0 \\ \Omega_F^*(t)/2 & \Delta_F(t)/2 & 0 \\ 0 & 0 & 2\delta+\Delta(t)/2 \end{bmatrix} \quad (12)$$

with the effective coupling Ω_F and detuning Δ_F of the coupled two-level system ($|e_+\rangle$ and $|e_-\rangle$), defined by

$$\Omega_F(t)=-\mathrm{Re}(\Omega_h)\cos 2\vartheta - i\,\mathrm{Im}(\Omega_h), \quad (13)$$

$$\Delta_F(t)=\sqrt{\Omega_m^2+\Delta^2}-\mathrm{Re}(\Omega_h)\sin 2\vartheta. \quad (14)$$

Note that similar coupling and detuning terms are discussed in the context of the zero-area pulse interaction with a two-level system [25].

The phase of $\Omega_F(t)$ in Eq. (13) is time dependent, so the dynamics can be better explained in the interaction picture. Figure 2(a) shows the numerical calculation of the coupling $|\Omega_F(t)|$ and the detuning $\Delta'_F(t)=\Delta_F(t)+d\ \arg[\Omega_F(t)]/dt$ in the interaction picture. Their plateau region around $t=\gamma$, the first (nonadiabatic) crossing point, manifests a near-resonant two-state coupling, which results in the complete population inversion ($|e_0\rangle\rightarrow|e_1\rangle$, $|e_1\rangle\rightarrow|e_0\rangle$) in the adiabatic basis, as shown in Fig. 2(b). When the system evolves further to the second crossing point (at which the adiabaticity is satisfied), the state $|e_1\rangle$ continues to remain in $|e_1\rangle$. So the given three-level system results in a closed two-level system, $|0\rangle$ and $|2\rangle$, in the bare-atom basis, plus an isolated state $|1\rangle$.

Figure 2(c) shows the fully numerical calculation of the final state populations in the bare-atomic basis using the Hamiltonian in Eq. (7) which includes the nonadiabatic coupling term, where Θ_0 is the pulse area of the calibrated transform-limited pulse having the same energy of the total pulse, defined by $\Theta_0=(2\mu/\hbar)(2\pi/\Delta\omega_m^2)^{1/4}\sqrt{\int|E(t)|^2dt}$. As the pulse energy increases, the state $|0(t=-\infty)\rangle$ either remains in $|0(t=\infty)\rangle$ (in the fully nonadiabatic regime for small Θ_0), or evolves to $|2(t=\infty)\rangle$ (in the hybrid adiabatic-nonadiabatic regime for in-between Θ_0), or to $|1(t=\infty)\rangle$ (in the fully adiabatic regime for large Θ_0). The result indicates the selective transitions to any energy state of the three-level system (i.e., $|0\rangle\rightarrow|0\rangle$,

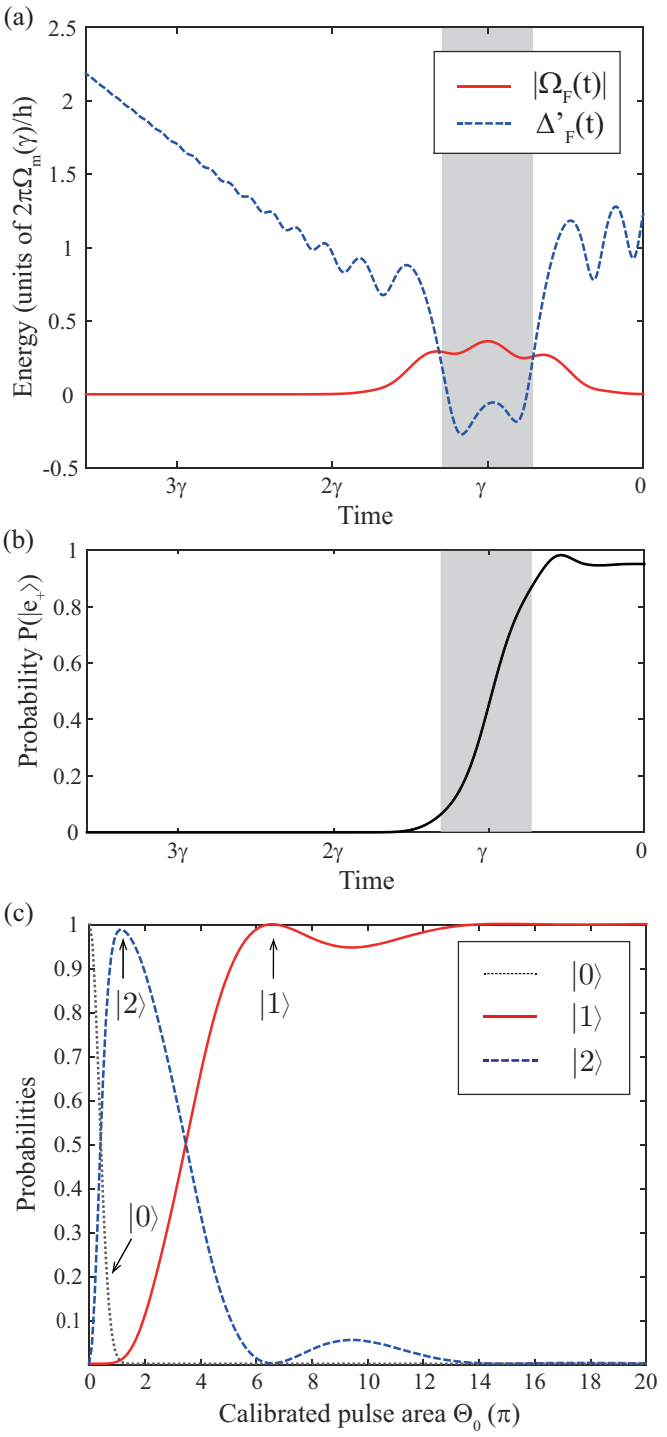

FIG. 2. (a) The effective coupling and detuning, defined in Eqs. (13) and (14), of the coupled two-level system. (b) The probability of the adiabatic energy state $|e_+\rangle$. (c) Probabilities of the bare energy states vs calibrated pulse area Θ_0 (see the text for the definition).

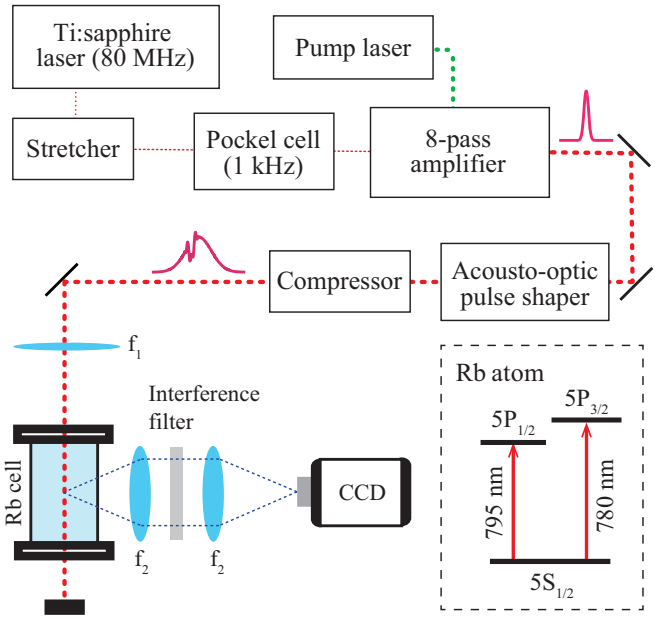

FIG. 3. Schematic experimental setup.

$|1\rangle$, or $|2\rangle$), controlled with only laser intensity (in the hybrid adiabatic-nonadiabatic coupling regime).

III. EXPERIMENTAL PROCEDURE

The experimental setup is schematically shown in Fig. 3. We used ultrashort optical pulses from a Ti:sapphire laser amplifier (homemade) operating with a repetition rate of 1 kHz and a pulse energy up to 25 μJ. The spectral bandwidth, the full width at half maximum, was 30 nm. The center wavelength was tuned to $\lambda = 787.6$ nm ($\omega_m = 2\pi c/\lambda$), the center between the transitions to $5P_{1/2}$ and $5P_{3/2}$ energy levels from the ground state $5S_{1/2}$ of atomic rubidium (^{85}Rb). Each laser pulse was programed with an acousto-optic pulse shaper (AOPDF, Dazzler from Fastlite) [27]. The spectral hole was centered at the transition to $5P_{1/2}$, and the linear chirp was varied from $c_2 = -20\,000$ to $50\,000$ fs^2 with the AOPDF. The spectral widths of the main and hole pulses were $\Delta\omega_m = (2\pi)9$ THz and $\Delta\omega_h = (2\pi)0.9$ THz, respectively. The depth of the spectral hole, α, was varied from zero to maximum, $\exp[-(\omega_h - \omega_m)^2/\Delta\omega_m^2]$, which is the spectral amplitude of the main pulse at the hole position. The shaped laser pulse was then focused with an $f_1 = 1000$ mm lens to atoms in a vapor cell of about 10^{12}/cm^3 density, and the fluorescence of the atoms induced by the pulse was measured with a CCD (Retiga 3000) through a two-lens relay imaging system with $f_2 = 50$ mm. We used two interference bandpass filters centered at 780 and 794.7 nm, respectively, to measure the fluorescence from the two excited levels, $5P_{1/2}$ and $5P_{3/2}$. The filters had a spectral bandwidth of 3 nm and 50% center transmittance.

IV. RESULTS AND DISCUSSION

Figure 4 compares the numerical calculation [(a1)–(a3), (b1)–(b3)] with the experimental results [(c1)–(c3), (d1)–(d3)]. The population difference between the excited states, $\Delta P = P(|1\rangle) - P(|2\rangle)$, is plotted for three chirp parameters: $c_2 = 50\,000$ fs^2 (the minimal hole-pulse condition, the first column), $20\,000$ fs^2 (a long hole-pulse condition, the second column), and $-20\,000$ fs^2 (a negative chirp, the third column). The numerical calculation in Figs. 4(a1), 4(a2), and 4(a3) shows the chirp-dependent behavior of the given hybrid adiabatic-nonadiabatic interaction. Under the minimal hole-pulse condition in Fig. 4(a1), a near-zero detuning ($\omega_h \approx \omega_1$) exhibits the as-expected intensity dependence of the selective excitation: As the pulse area (Θ_0) increases, the state evolves to $|2\rangle$ or $|1\rangle$ in the region marked by ① or ②, respectively. Near ①, the system evolves to $|2\rangle$ through the hybrid adiabatic-nonadiabatic interaction. However, when the adiabatic condition is fully satisfied around ②, the system evolves to $|1\rangle$. Note that the region near ③ is the case for a large hole detuning; this region exhibits an ordinary chirped-RAP behavior, because in this case the far-off-resonant hole plays little role in the overall dynamics. The long hole-pulse case, in Fig. 4(a2), shows an extended nonadiabatic coupling near both the first and second adiabatic crossing points; thus, the overall dynamics appears sensitively dependent on both the hole detuning and the pulse area, as expected. In the negative chirp case, in Fig. 4(a3), the hole pulse is colocated with the second adiabatic crossing point, resulting in, again, an ordinary chirped RAP (to $|2\rangle$ in this case because of the negative sign of the chirp), irrespective of the hole detuning.

The second row of Fig. 4 is the spatially averaged calculation of the first row. Because the laser beam has a Gaussian spatial profile in the transverse direction, each atom in the ensemble interacts with a different laser intensity [28]. The Gaussian beam radius of 250 μm and the Rayleigh range of about 20 cm greatly exceed the size (about 50 μm) of the imaged area. When this spatial average effect due to the transverse laser beam profile is taken into account, the numerical calculation results in Figs. 4(b1), 4(b2), and 4(b3), showing good agreement with the experimental result in the third row, Figs. 4(c1), 4(c2), and 4(c3), respectively.

The spatially averaging process from the first row to the second can be represented in terms of the pulse area as $P_{\rm avg}(\Theta_0) = \int_0^{\Theta_0} P(\Theta_0')A(\Theta_0,\Theta_0')d\Theta_0'$, so an inverse matrix calculation from $P_{\rm avg}(\Theta_0)$ to $P(\Theta_0)$ is allowed (because A is a triangular matrix with nonzero diagonal components, thus, having nonzero determinant). When the inverse matrix calculation from the third row is performed (after a coarse graining), the result is as shown in the fourth row, which is the unaveraged population difference retrieved from experimental data. In particular, the result in Fig. 4(d1) apparently shows the anticipated intensity-dependent selective excitation, in good agreement with Fig. 4(a1).

Figure 5 shows the contribution of the hole depth to the given selective excitation scheme. A chirped pulse without a hole, which is the case of zero hole depth, or $\alpha = 0$ [defined in Eq. (1)], simply makes usual chirped RAP, so the excited population only goes to $|1\rangle$. If α increases from zero (no hole) to maximum (the maximal hole), the the population excited to $|2\rangle$ increases from zero (no $|2\rangle$ excitation) to one (fully excited $|2\rangle$). If we define the degree of inversion $T(\alpha) = |\Delta P_{\rm min}(\alpha)/\Delta P_{\rm min}(\alpha = 1.0)|$, where $\Delta P_{\rm min}$ is the minimal population difference ΔP for a given hole depth α during the entire evolution, $T(\alpha)$ quantifies the selective

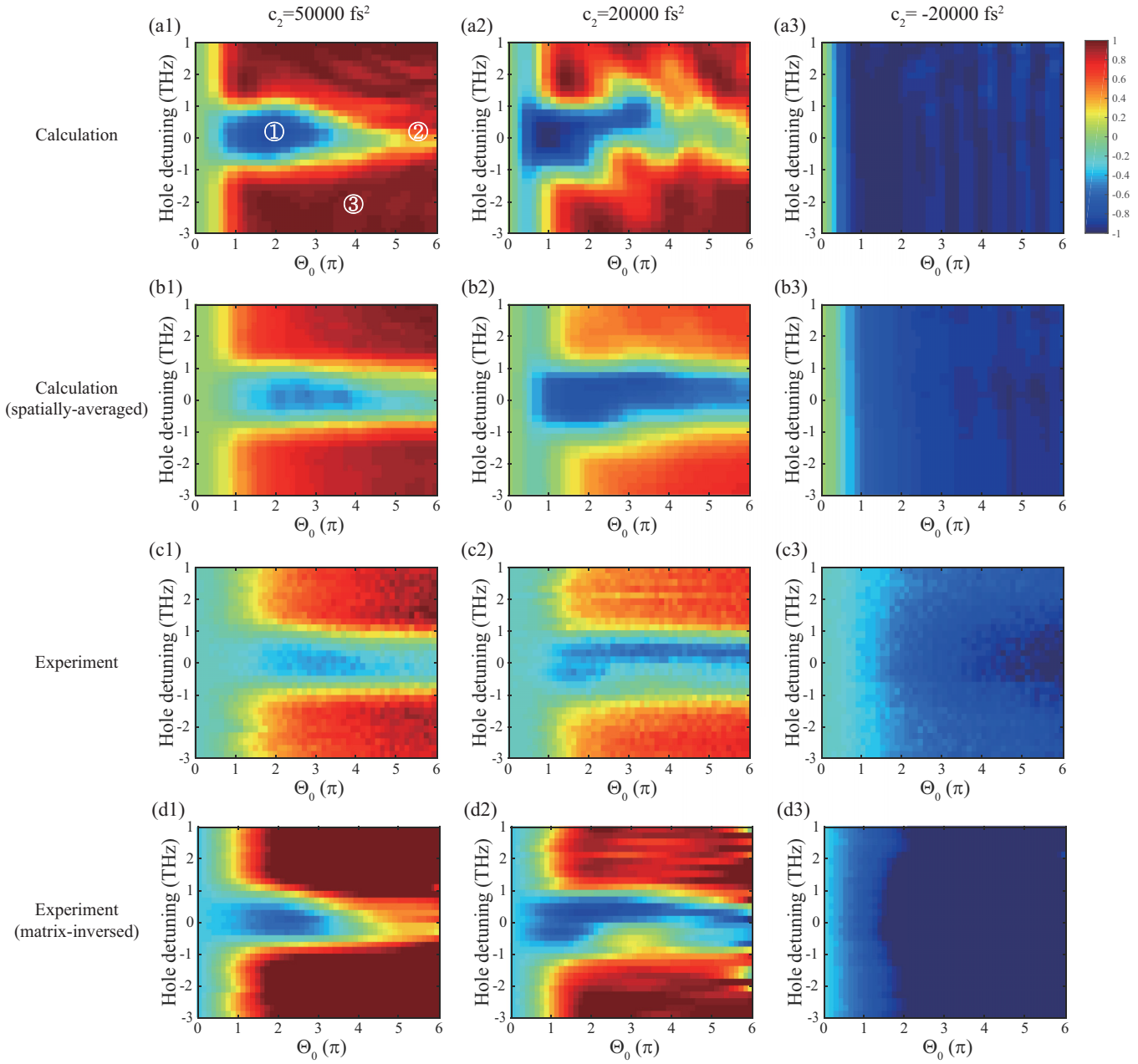

FIG. 4. Population difference, $\Delta P = P(|1\rangle) - P(|2\rangle)$, plotted as a function of the hole detuning, $\delta_h = \omega_h - \omega_1$, and the calibrated pulse area Θ_0: (a) calculation without the spatial-average consideration, (b) calculation with the spatial-average consideration, (c) experimental results, and (d) experimental results retrieved through the inverse calculation of spatial averaging. The left column [(a1), (b1), (c1), (d1) corresponds to $c_2 = 50\,000$ fs^2 (the minimal hole-pulse width condition), the middle column [(a2), (b2), (c2), (d2)] $c_2 = 20\,000$ fs^2 (a long hole pulse), and the right column [(a3), (b3), (c3), (d3)] $c_2 = -20\,000$ fs^2 (a negatively chirped pulse). The color scheme of the figures indicates the final ($t = \infty$) state of the system to be in either $|2\rangle$ (blue) or $|1\rangle$ (red).

excitation ($T = 0$ for $|0\rangle \rightarrow |1\rangle$ and $T = 1$ for $|0\rangle \rightarrow |2\rangle$). Experiment was performed with laser power varied up to 25 μJ (which corresponds to 6π in pulse area) and a fixed chirp parameter $c_2 = 50\,000$ fs^2. The result in Fig. 5 shows that, when the depth was large, $\alpha \approx \exp[-(\omega_h - \omega_m)^2/\Delta\omega_m^2]$, enough to completely remove the spectrum at ω_h, the ground state evolved to the second excited state (i.e., $|0\rangle \rightarrow |2\rangle$), and that no hole ($\alpha = 0$) induced the ordinary chirped RAP, a cyclic permutation of the energy states, in good agreement with the theoretical analysis. The degree of inversion $T(\alpha)$ was calculated from the experimental data using two methods: the first method simply assumed a Gaussian fluorescence spot to deal with the background noise and the second eliminated the background noise under the assumption of monotonic polynomial dependence with respect to the pulse area. As expected, the result obtained with the second method agrees well with the theoretical calculation.

We now turn our attention to the implications of the results obtained in this study to possible applications. The first example is the closed adiabatic two-excited-state transitions

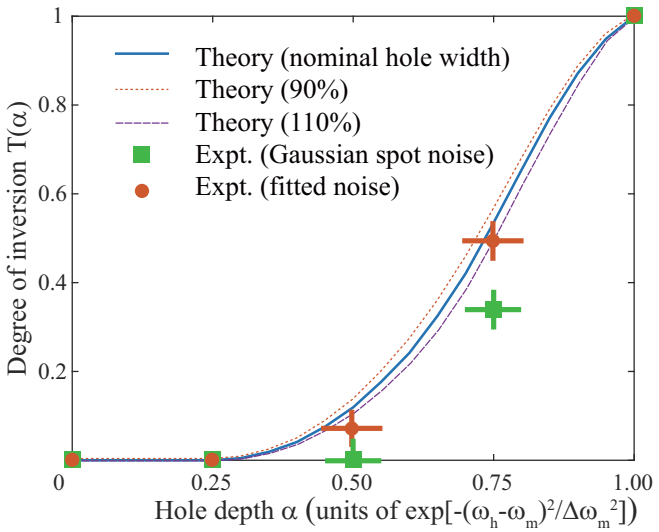

FIG. 5. The degree of inversion $T(\alpha) = |\Delta P_{\min}(\alpha)/\Delta P_{\min}(\alpha = 1.0)|$ vs the hole depth α. Theoretical lines are calculated with three different hole widths; nominal (blue solid line), 90% (orange dotted line), and 110% (purple dashed line). Experimentally retrieved values for $T(\alpha)$ are shown with circles (Gaussian spot noises) and squares (polynomial fitted noise). (See the text for more details.)

$|1\rangle \leftrightarrow |2\rangle$, which can be made by combining the given hybrid interaction and an ordinary chirped RAP (with a negative chirp): Since an ordinary negatively chirped RAP induces the cyclic state permutations, a subsequent hybrid interaction $|0\rangle \leftrightarrow |2\rangle$ completes an adiabatic exchange of the excited states, $|1\rangle \leftrightarrow |2\rangle$, and $|0\rangle$ is unchanged. Therefore, with this procedure, an ultrafast time-scale adiabatic control among the excited states of a V-type three-level system may be achieved. In particular, our control method of a Raman-coupled two-level system may be applied similarly to the ground-state two-levels in a λ-type system that is often used as a long-storage qubit. The second example is an optical control of N qubits arranged in a lattice [29,30]. In particular, when a short lattice constant makes a conventional optics with focused beams difficult to address individual qubits, our method may provide a solution: Our calculation (not shown) predicts that spatial beam-shape profiling in conjunction with the given intensity-dependent selective excitation achieves subwavelength-scale qubit controls. For example, the atomic qubit gates constructed based on the Rydberg-atom dipole blockade effect often use about 10-μm-scale optical microtraps [31–33], so reducing the lattice constant down below one wavelength allows one to use significantly lower Rydberg energy states, which may be useful for faster quantum gate operations.

V. CONCLUSION

In summary, we have shown that a chirped laser pulse with a spectral hole can turn on or off an adiabatic crossing point of the conventional chirped RAP of a three-level system in the V-type configuration. This result suggests that our method, being combined with the ordinary chirped RAP, implements an adiabatic transitions between the two excited states. Experiments performed with shaped femtosecond laser pulses and the three lowest energy levels ($5S_{1/2}$, $5P_{1/2}$, and $5P_{3/2}$) of atomic rubidium have shown good agreement with the theoretically analyzed dynamics of the three-level system. The programed hybrid adiabatic-nonadiabatic interaction allows three-level system control by laser intensity only, which may have applications including selective excitations of atoms or ions arranged in space in conjunction with laser beam profile programming.

ACKNOWLEDGMENT

This research was supported by Samsung Science and Technology Foundation (SSTF-BA1301-12).

[1] B. W. Shore, *Manipulating Quantum Structures Using Laser Pulses* (Cambridge University Press, New York, 2011).
[2] M. A. Nielsen and I. L. Chuang, *Quantum Computation and Quantum Information* (Cambridge University Press, New York, 2010).
[3] D. Goswami, Laser Phase Modulation Approaches Towards Ensemble Quantum Computing, Phys. Rev. Lett. **88**, 177901 (2002).
[4] Y. Liang, Q.-C. Wu, S.-L. Su, X. Ji, and S. Zhang, Shortcuts to adiabatic passage for multiqubit controlled-phase gate, Phys. Rev. A **91**, 032304 (2015).
[5] H. Goto and K. Ichimura, Multiqubit controlled unitary gate by adiabatic passage with an optical cavity, Phys. Rev. A **70**, 012305 (2004).
[6] Z. Kis and F. Renzoni, Qubit rotation by stimulated Raman adiabatic passage, Phys. Rev. A **65**, 032318 (2002).
[7] B. Rousseaux, S. Gúerin, and N. V. Vitanov, Arbitrary qudit gates by adiabatic passage, Phys. Rev. A **87**, 032328 (2013).
[8] D. D. Bhaktavatsala Rao and K. Mølmer, Robust Rydberg-interaction gates with adiabatic passage, Phys. Rev. A **89**, 030301(R) (2014).
[9] S. B. Zheng, Nongeometric Conditional Phase Shift Via Adiabatic Evolution of Dark Eigenstates: A New Approach to Quantum Computation, Phys. Rev. Lett. **95**, 080502 (2005).
[10] N. V. Vitanov, T. Halfmann, B. W. Shore, and K. Bergmann, Laser-induced population transfer by adiabatic passage techniques, Annu. Rev. Phys. Chem. **52**, 763 (2001).
[11] J. S. Melinger, S. R. Gandhi, A. Hariharan, J. X. Tull, and W. S. Warren, Generation of Narrowband Inversion with Broadband Laser Pulses, Phys. Rev. Lett. **68**, 2000 (1992).
[12] R. Netz, T. Feurer, G. Roberts, and R. Sauerbrey, Coherent population dynamics of a three-level atom in spacetime, Phys. Rev. A **65**, 043406 (2002).
[13] K. Bergmann, H. Theuer, and B. W. Shore, Coherent population transfer among quantum states of atoms and molecules, Rev. Mod. Phys. **70**, 1003 (1998).

[14] A. Ruschhaupt and J. G. Muga, Adiabatic interpretation of a two-level atom diode, a laser device for unidirectional transmission of ground-state atoms, Phys. Rev. A **73**, 013608 (2006).
[15] M. Garwood and L. DelaBarre, The return of the frequency sweep: Designing adiabatic pulses for contemporary NMR, J. Magn. Reson. **153**, 155 (2001).
[16] L.-M. Duan, A. Kuzmich, and H. J. Kimble, Cavity QED and quantum-information processing with "hot" trapped atoms, Phys. Rev. A **67**, 032305 (2003).
[17] K. S. Kumar, A. Vepsäläinen, S. Danilin, and G. S. Paraoanu, Stimulated Raman adiabatic passage in a three-level superconducting circuit, Nat. Commun. **7**, 10628 (2016).
[18] A. Debnath, C. Meier, B. Chatel, and T. Amand, Chirped laser excitation of quantum dot excitons coupled to a phonon bath, Phys. Rev. B **86**, 161304(R) (2012).
[19] A. M. Weiner, *Ularafast Optics* (Wiley, Hoboken, 2009).
[20] A. M. Weiner, Ultrafast optical pulse shaping: A tutorial review, Opt. Commun. **284**, 3669 (2011).
[21] N. Dudovich, T. Polack, A. Pe'er, and Y. Silberberg, Simple Route to Strong-Field Coherent Control, Phys. Rev. Lett. **94**, 083002 (2005).
[22] T. Bayer, M. Wollenhaupt, C. Sarpe-Tudoran, and T. Baumert, Robust Photon Locking, Phys. Rev. Lett. **102**, 023004 (2009).
[23] S. Lee, H. G. Lee, J. Lim, J. Cho, C. Y. Park, and J. Ahn, Coherent control of multiphoton-ionization passage of excited-state rubidium atoms, Phys. Rev. A **86**, 045402 (2012).
[24] H. G. Lee, H. Kim, J. Lim, and J. Ahn, Quantum interference control of four-level diamond-configuration quantum system, Phys. Rev. A **88**, 053427 (2013).
[25] H. G. Lee, Y. Song, H. Kim, H. Jo, and J. Ahn, Quantum dynamics of a two-state system induced by a chirped zero-area pulse, Phys. Rev. A **93**, 023423 (2016).
[26] M. Wollenhaupt, T. Bayer, N. V. Vitanov, and T. Baumert, Three-state selective population of dressed states via generalized spectral phase-step modulation, Phys. Rev. A **81**, 053422 (2010).
[27] P. Tournois, Acousto-optic programmable dispersive filter for adaptive compensation of group delay time dispersion in laser systems, Opt. Commun. **140**, 245 (1997).
[28] H. G. Lee, H. Kim, and J. Ahn, Ultrafast laser-driven Rabi oscillations of a Gaussian atom ensemble, Opt. Lett. **40**, 510 (2015).
[29] J. Beugnon, C. Tuchendler, H. Marion, A. Gaëten, Y. Miroshnychnko, T. R. P. Sortais, A. M. Lance, M. P. A. Jones, G. Messin, A. Browaeys, and P. Grangier, Two-dimensional transport and transfer of a single atomic qubit in optical tweezers, Nat. Phys. **3**, 696 (2007).
[30] R. Blatt and D. J. Wineland, Entangled states of trapped atomic ion, Nature (London) **453**, 7198 (2008).
[31] M. J. Piotrowicz, M. Lichtman, K. Maller, G. Li, S. Zhang, L. Isenhower, and M. Saffman, Two-dimensional lattice of blue-detuned atom traps using a projected Gaussian beam array, Phys. Rev. A **88**, 013420 (2013).
[32] F. Nogrette, H. Labuhn, S. Ravets, D. Barredo, L. Béguin, A. Vernier, T. Lahaye, and A. Browaeys, Single-Atom Trapping in Holographic 2D Arrays of Microtraps with Arbitrary Geometries, Phys. Rev. X **4**, 021034 (2014).
[33] W. Lee, H. Kim, and J. Ahn, Three-dimensional rearrangement of single atoms using actively controlled optical microtraps, Opt. Express **24**, 9816 (2016).